Geophysical Research Letters

RESEARCH LETTER
10.1029/2018GL079884

Key Points:
- Compared to realistic models without tides, baroclinic tides induce 2-3 times larger horizontal and vertical dispersion
- Three-dimensional drifter tracking is important for passive tracer dispersion

Correspondence to:
S. H. Suanda,
ata.suanda@otago.ac.nz

Citation:
Suanda, S. H., Feddersen, F., Spydell, M. S., & Kumar, N. (2018). The effect of barotropic and baroclinic tides on three-dimensional coastal dispersion. *Geophysical Research Letters*, *45*. https://doi.org/10.1029/2018GL079884

Received 4 AUG 2018
Accepted 25 SEP 2018
Accepted article online 28 SEP 2018

The Effect of Barotropic and Baroclinic Tides on Three-Dimensional Coastal Dispersion

Sutara H. Suanda[1], Falk Feddersen[2], Matthew S. Spydell[2], and Nirnimesh Kumar[3]

[1]Department of Marine Science, University of Otago, Dunedin, New Zealand, [2]Scripps Institution of Oceanography, San Diego, CA, USA, [3]Civil and Environmental Engineering, University of Washington, Seattle, WA, USA

Abstract The effects of barotropic and baroclinic tides on three-dimensional (3-D) coastal dispersion are examined with realistic, 200-m horizontal resolution simulations of the Central Californian continental shelf during upwelling. Over multiple tidal cycles, the horizontal relative dispersion and vertical dispersion of 3-D drifters are similar between simulations with no tides and with barotropic tides. In contrast, baroclinic tides, which dissipate across the shelf and induce vertical mixing, result in a factor of 2–3 times larger horizontal and vertical dispersion. The increase in horizontal dispersion with vertical mixing is qualitatively consistent with weak-mixing shear dispersion. Without shear dispersion, horizontal dispersion of surface-trapped (2-D) drifters was similar in all simulations. However, 2-D drifter trajectory differences relative to no tide simulations are 3–4 times larger with baroclinic tides than barotropic tides alone. These results demonstrate the need to include baroclinic tides and 3-D tracking for coastal passive tracer dispersion.

Plain Language Summary Understanding the dispersal of material in the coastal ocean is relevant to pollutant dilution, marine ecosystem sustainability, and search-and-rescue operations. Although numerical circulation models are commonly used to predict material dispersal, these models often do not include tides. Here the tidal effect on material dispersal is compared with numerical drifters released in a realistic model without tides, with surface tides (the rise and fall of sea level), and with internal tides (the rise and fall of interior density layers). Surface tides contribute little additional dispersal in the model region, while internal tides induce 2–3 times larger horizontal and about 2 times larger vertical dispersal in comparison to models without tides. In addition, after 48 hr surface drifter trajectory differences between models with and without internal tides are 8 km. Therefore, internal tides need to be considered in models used to plan oil-spill response or search-and-rescue operations.

1. Introduction

Tracer dispersion in the coastal ocean has wide reaching impacts on pollutants (e.g.,Boehm et al., 2002; Macfadyen et al., 2011; Poje et al., 2014), search-and-rescue operations (e.g., Spaulding et al., 2006), the exchange of iron and nutrients (e.g., McPhee-Shaw, 2006), and the connectivity of marine organisms (e.g., Cowen & Sponaugle, 2009; Monismith et al., 2018; Pineda et al., 2007). Lagrangian analysis of surface-trapped drifters (e.g., Davis, 1985; Ohlmann et al., 2012; Spydell et al., 2009), dye releases (e.g., Clark et al., 2010; Dale et al., 2006; Hally-Rosendahl et al., 2014; Moniz et al., 2014; Sundermeyer & Ledwell, 2001), and virtual drifter tracking with high-frequency radar velocities (e.g., Rypina et al., 2016) provide estimates of dispersal patterns and dispersion rates at different space and time scales that inform coastal resource management. Due to limited Lagrangian observations, marine connectivity (Drake et al., 2011; Mitarai et al., 2009; Petersen et al., 2010) and pollutant dispersion (e.g., Thyng & Hetland, 2017) are also estimated by virtual drifters advected with realistic numerical models. The broad range of space and time scales from the nearshore (O(10) m and O(1) min) to the outer continental shelf (O(10) km, O(1) day) also present a challenge to coastal numerical modeling. Regional operational models such as those from Integrated Ocean Observing Systems (https://ioos.noaa.gov/) can well represent wind-driven and mesoscale dynamics (e.g., Veneziani et al., 2009) but typically have relatively coarse horizontal resolution (O(1–3) km) and poorly resolve continental shelf circulation from the shoreline to 100-m water depth (e.g., Drake et al., 2011; Mitarai et al., 2009). Both U.S. West Coast wide dispersal study with a 3-km resolution model (Drake et al., 2011) and regional study with a 1-km resolution model (Mitarai et al., 2009) describe the effects of large space scale (> 10 km) and long time scale (> 10 day) dispersion processes. Because < 1-km spatial scales within a model can impact coastal dispersion estimates

(e.g., Bracco et al., 2018; Rasmussen et al., 2009), these processes can be resolved by further model nesting (e.g., Romero et al., 2013), parameterized within the Lagrangian submodel (e.g., Lacorata et al., 2014; Rypina et al., 2016) or resolved with an unstructured model grid (e.g., Rayson et al., 2016). For oil-spill response applications, or to compare with near-surface trapped drifter observations, some model-based dispersion studies focus on near-surface horizontal (two-dimensional, 2-D) dispersion (e.g., Ohlmann & Mitarai, 2010; Romero et al., 2013; Thyng & Hetland, 2017). Nonbuoyant tracers such as pollutants, nutrients, and larvae are transported and mixed in coastal regions by the full three-dimensional (3-D) flow field that includes turbulent boundary layers, interior internal tide-driven mixing, as well as geostrophic flows, which potentially impact horizontal and vertical tracer dispersion.

Many previous U.S. West Coast model-based dispersion studies have not included tides (e.g., Drake et al., 2011; Kim & Barth, 2011; Mitarai et al., 2009). Although hindcast (Kurapov et al., 2017) and operational models (Chao et al., 2017) of the region have recently incorporated tides, dispersion studies with realistic models that incorporate tides remain limited (e.g., Romero et al., 2013). Barotropic (BT; surface) and baroclinic (BC; internal) tides potentially impact dispersion through processes including BT tidal rectification (e.g., Ganju et al., 2011), internal wave shear dispersion (Kunze & Sundermeyer, 2015; Steinbuck et al., 2011; Young et al., 1982), and internal wave Stokes' Drift (Wunsch, 1971).

In realistic coastal models, the importance of including BT and BC tides relative to coastal processes driven by winds, stratification, and bathymetric variability on tracer dispersion is not well understood. In a study using a high-resolution (250-m grid spacing) coastal model that included BT and BC tides, horizontal dispersion was due to a combination of submesoscale processes and tides (Romero et al., 2013). However, no distinction between BT and BC tidal effects was made and no direct comparison of dispersal rates or drifter trajectories between models that include and neglect tides was provided. About 10% of the global energy input to BC tides (0.1 TW) is eventually dissipated on the continental shelf (e.g., Kelly et al., 2013) and observations of elevated coastal vertical mixing have been linked to BC tides (e.g., MacKinnon & Gregg, 2003; Walter et al., 2012). Thus, BC tides may have a strong effect on coastal stratification and dispersion. The effect of BT and BC tides on middle to inner- shelf stratification and vertical mixing was examined using three Central California (U.S. West Coast) simulations with identical realistic wind and large-scale boundary conditions but with either no tides (NT), BT only tides, or both BT and BC tides (Suanda et al., 2017). Tidal effects were isolated by analysis of a time period with similar volume-averaged heat content and upwelling mean flows in the three simulations. Relative to simulations without BC tides, the onshore-propagating, dissipating BC tide increased midwater column vertical mixing and reduced subtidal stratification with comparable magnitude to the observed natural seasonal cycle (Suanda et al., 2017).

Here in this follow-up study utilizing the same simulations, the potential enhanced drifter dispersion due to BT and BC tides over multiple tidal time scales relative to a simulation without tides is examined. The primary metric to characterize horizontal drifter dispersion is the time-dependent relative diffusivity (e.g., Richardson, 1926; Salazar & Collins, 2009; Sawford, 2001), which has been used previously in coastal regions (e.g., Ohlmann et al., 2012; Romero et al., 2013; Spydell & Feddersen, 2009). In homogeneous and isotropic turbulence, the relative diffusivity is understood to be time dependent as long as drifter separations are shorter than the largest eddy scales (e.g., Jullien et al., 1999; Salazar & Collins, 2009) and times shorter than the Lagrangian time scale of absolute diffusivity (e.g., Taylor, 1922). In coastal regions, the Lagrangian time scale has been estimated to be multiple days (e.g., Davis, 1985; Dever et al., 1998; Paduan & Niiler, 1993). As this is longer than semidiurnal time scales, the effects of BC and BT tides on time-dependent drifter relative dispersion are examined here.

The model setup, drifter tracking methods, and Lagrangian statistics are described in section 2. Horizontal and vertical dispersion statistics in the NT, BT tides, and BC tides simulations are compared in section 3. The mechanisms inducing additional vertical and horizontal dispersion with BC tides, the differences between 3-D and 2-D dispersion, and the trajectory difference between simulations are discussed in section 4. Results are summarized in section 5.

2. Model and Methods

2.1. ROMS Simulations

Realistic continental shelf hydrodynamics within the Central Californian coastal upwelling system are simulated with ROMS (Regional Ocean Modeling System), a nonlinear, three-dimensional, terrain-following, open

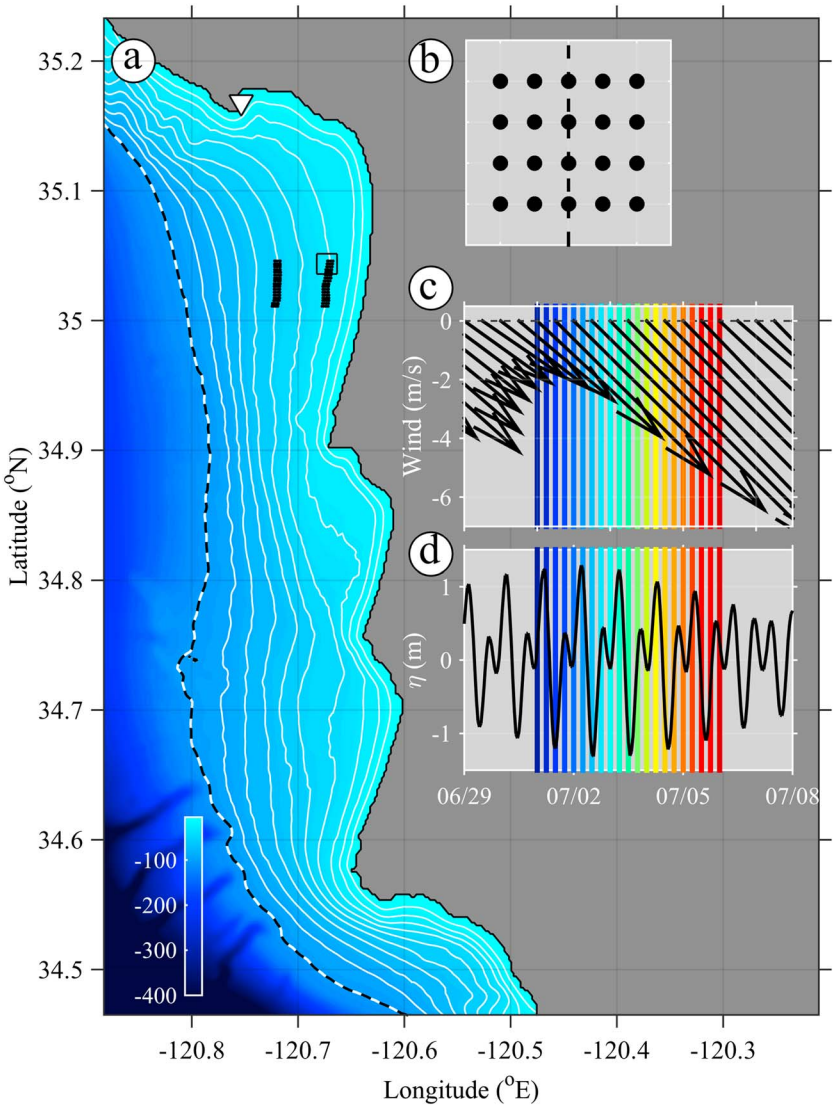

Figure 1. (a) Continental shelf model domain. Bathymetry is contoured in white curves in 10-m increments with the 100-m isobath highlighted by the black and white curves. Black dots denote release locations of near-surface drifters along the 30- and 50-m isobaths. White triangle denotes location of the Port San Luis (SLO) tide gauge. (b) Schematic of a portion of the drifter release pattern expanded from black square in panel (a). The dashed line is the release isobath, and each black dot is the release location at three vertical levels ($z = -1, -2, -3$ m). (c) Regional model winds and (d) modeled sea surface elevation versus time at SLO. In (c) and (d), vertical line colors indicate drifter release times (separated by 6 hr) between 1 July (dark blue) and 6 July (dark red).

source numerical model that solves the Reynolds-averaged Navier-Stokes equations with hydrostatic and Boussinesq approximations (Haidvogel et al., 2008; Shchepetkin & McWilliams, 2005; Warner et al., 2010). The ROMS setup is briefly described here with further details in Suanda et al., (2016, 2017). Three levels of offline nesting (downscaling) transmit large-scale variability through open boundary conditions from a U.S. West Coast-wide ocean simulation to a continental shelf domain (e.g., Marchesiello et al., 2001; Mason et al., 2010; Suanda et al., 2017). The shelf domain is about 80 km by 25 km wide, with a horizontal grid spacing of 200 m and 42 vertical levels (Figure 1). The k-ϵ turbulence closure model represents subgrid vertical mixing and gives the time- and space-varying vertical eddy diffusivity k_V (e.g., Umlauf & Burchard, 2005; Warner et al., 2005). It is a standard turbulence model for coastal application (e.g., Durski et al., 2004; Wijesekera et al., 2003) and represents well the dissipating BC tide (Kumar et al., 2015). All levels of nesting use the same realistic COAMPS daily-averaged atmospheric forcing with ≈ 9-km resolution (Hodur et al., 2002). The model is run for 60 days from 1 June to 31 July 2000.

Three continental shelf simulations are conducted. The first has no BT or BC tides (referred to as NT). A second simulation includes BT tides (local tides, LT) by adding harmonic sea level and BT velocity of eight astronomical semidiurnal and diurnal tidal constituents and two overtides from the ADCIRC Tidal Constituent Database for the Eastern North Pacific Ocean (e.g., Mark et al., 2004) to the domain open boundaries (Figure 1a). BT tides are accurately simulated with this model setup (Suanda et al., 2016). The third simulation has both BT and BC tides (with tides, WT), inheriting boundary conditions with the addition of the ADCIRC BT tidal forcing applied on the prior level of nesting. BT-to-BC tidal conversion within the larger domain result in a net onshore, remotely generated, semidiurnal internal tide energy flux of $\approx$ 100 W/m on the boundary of the continental shelf domain (Suanda et al., 2017). In WT (including BT and BC tides), frequency spectra of midwater column temperature and surface cross-shore velocity were comparable to observations (Suanda et al., 2017).

2.2. Lagrangian drifter tracking

In the three simulations (NT, LT, and WT), virtual drifters are released and tracked with the offline Lagrangian TRANSport model (LTRANS) software package (North et al., 2006), utilizing the ROMS model three-dimensional (3-D) and time-dependent velocities and diffusivity. In the east-west (x) direction drifters are advected by

$$\frac{\delta x_i}{\delta t} = u + \left[\frac{2k_H}{\delta t}\right]^{1/2} R_n, \tag{1}$$

where x_i is the i-th drifter x position, u is the ROMS x velocity interpolated to drifter position, and $k_H = 1$ m^2/s is a constant random-walk horizontal diffusivity, chosen to be small relative to drifter-derived continental shelf diffusivity values of O(100 m^2/s) at spatial scales of 3–5 km (e.g., Romero et al., 2013). The LTRANS time step $\delta t = 120$ s and R_n is a normally distributed random number. LTRANS integrates (1) with a fourth-order Runga-Kutta scheme (North et al., 2006). The LTRANS time step of $\delta t = 120$ s is at least 2 orders of magnitude smaller than the tidal time scales that dominate initial drifter dispersion. In limited tests, bulk drifter dispersion statistics were very similar with a much shorter LTRANS time step $\delta t = 10$ s. North-south (y) drifter advection is analogous to (1). Vertical (z) drifter advection is given by

$$\frac{\delta z_i}{\delta t} = \left(w + \frac{\partial k_V}{\partial z}\right) + \left[\frac{2k_V}{\delta t}\right]^{1/2} R_n, \tag{2}$$

where the space- and time-dependent vertical diffusivity k_V from k-ϵ closure is interpolated to the drifter position. Because k_V varies in z, an additional term $\partial k_V/\partial z$ is included to account for Lagrangian advection to regions of high diffusivity (e.g., Davis, 1991; North et al., 2006; Schlag & North, 2012).

2.3. Drifter Releases

Upwelling favorable conditions are common during the summer in Central California. The specific 5-day time period of coastal upwelling was chosen as there was similar heat content across NT, LT, WT, and similar spatial-temporal mean current patterns (Suanda et al., 2017). Time-dependent model winds were from the northwest, increasing in intensity from $\approx$ 5 m/s to $\approx$ 10 m/s over the 5 days (Figure 1c). Model winds compare well to buoy observations at this location (Suanda et al., 2016). BT tides had a 2-m maximum tide range (Figure 1d) and were similar in LT and WT (Suanda et al., 2017). In each simulation, drifters are repeatedly released in two near-surface patches centered on the 30- and 50-m isobaths (black dots, Figure 1a) in regions of relative along-shore uniformity corresponding to the analysis region of Suanda et al. (2017). Each patch extends 500 m by $\approx$ 4 km by 2 m in the cross, along-isobath and vertical directions with release spacing of 125 and 200 m, respectively (Figure 1b). At each release location, drifters are released at $z = -1, -2, -3$ m below the tidally modulated sea surface. A total of 21 releases separated by $\Delta t = 6$ hr was conducted over the 5-day period resulting in 6,300 drifters in each patch. After release, drifters are tracked for four semidiurnal tidal cycles (48 hr) to quantify their initial spreading rates over multiple tidal cycles but before the longer-time dispersion processes that occur at larger separation (e.g., Davis, 1985). Drifters crossing land, sea surface, or bottom boundaries are specularly reflected. In 48 hr, $\approx$ 2% of released drifters leave the model domain and are only included in the analysis when within the domain.

2.4. Drifter Statistics

Bulk drifter relative dispersion rates are quantified by temporal growth in drifter position variance from the 30- and 50-m isobath releases, respectively. The time-staggered releases are recast into hours after release t

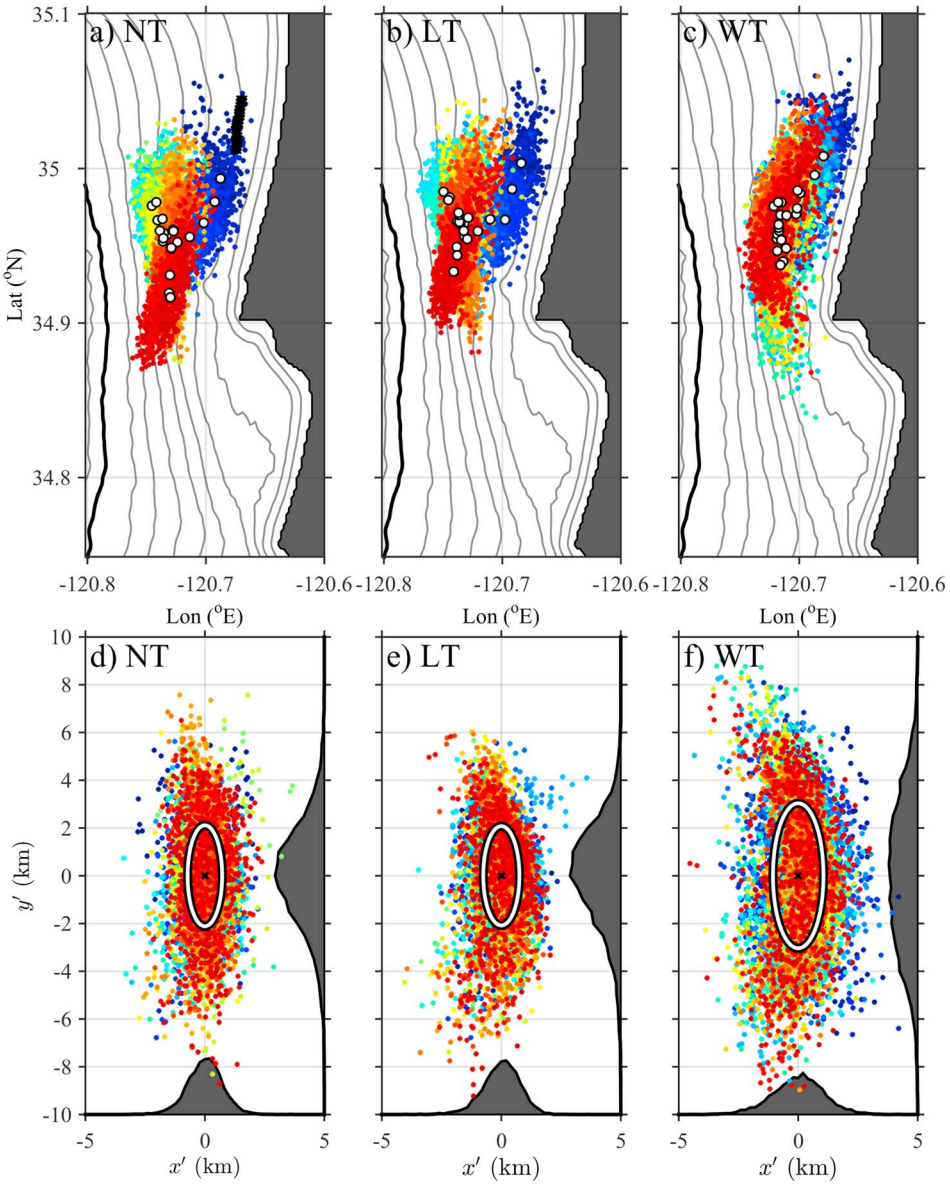

Figure 2. (a–c) Snapshot of all (n = 21) 30-m isobath drifter releases versus latitude and longitude at t = 30 hr after release in the (a) NT, (b) LT, and (c) WT simulations. Colors indicate release times (see Figures 1c and 1d). Each release center of mass is denoted by white circles. Black curve is the 100-m isobath, and drifter release locations are marked by the black strip in panel (a). (d–f) Snapshot of all 30-m isobath drifter releases in the principal axes coordinate system (x', y') at t = 30 h after release. The white ellipses indicate the horizontal dispersion ellipse with area D_E^2 (4). Dark shaded curves are the normalized probability distribution functions along each axes. NT = no tides; LT = local tides; WT = with tides.

(e.g., Davis, 1983). In the x direction, the patch relative dispersion D_{xx}^2 (e.g., LaCasce, 2008; Rypina et al., 2016) is

$$D_{xx}^2(t) = \left\langle (\Delta x(t) - \overline{\Delta x}_i(t))^2 \right\rangle, \tag{3}$$

where $\Delta x(t)$ is a drifter's east-west displacement from release location, $\overline{\Delta x}_i$ is the mean east-west displacement of all drifters in a release i (center of mass), and the ensemble average $\langle \cdot \rangle$ is over all drifters in a release and all 21 releases. An analogous expression to (3) is defined in the north-south (y) direction ($D_{yy}^2(t)$) and also for the cross-dispersion $D_{xy}^2(t)$. These D^2 components are used to define principal axes directions (x', y') such that $D_{y'y'}^2$ and $D_{x'x'}^2$ are the relative dispersion in the major and minor axes direction, respectively (e.g., Romero et al., 2013; Rypina et al., 2016; Sundermeyer & Ledwell, 2001). The principal axes dispersion defines a bulk horizontal relative dispersion ellipse with area (ensemble patch size),

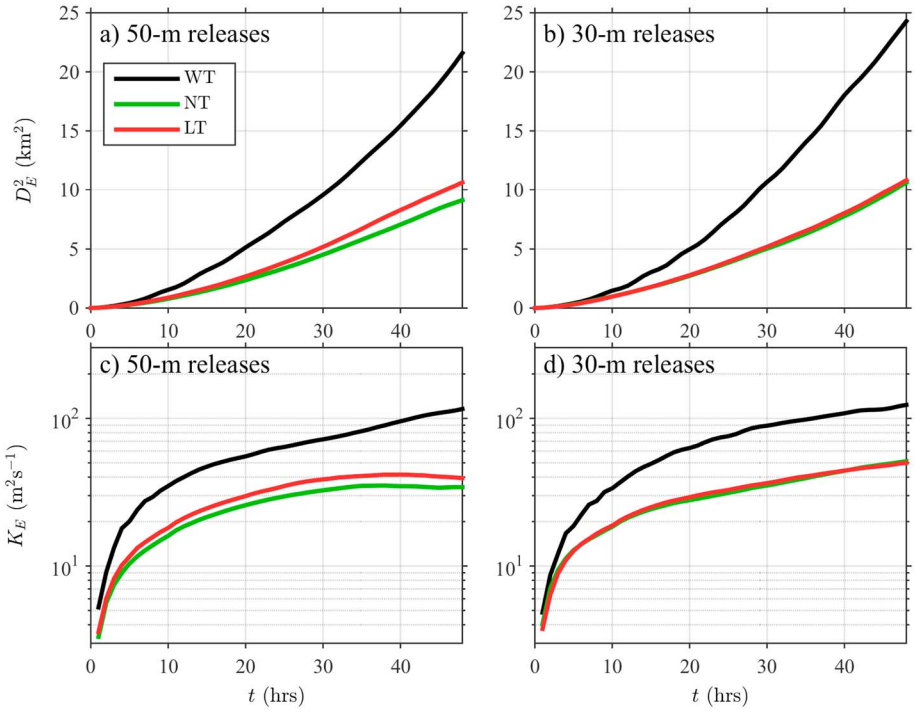

Figure 3. (a, b) Horizontal relative dispersion ellipse area D_E^2 (equation (4)) and (c, d) horizontal diffusivity K_E (equation (5)) versus time after release t for the (a, c) 50 and (b, d) 30-m isobath releases. The WT, NT, and LT simulations are indicated in legend (panel a). WT = with tides; NT = no tides; LT = local tides.

$$D_E^2(t) = \pi(D_{x'x'}^2, D_{y'y'}^2)^{1/2}. \tag{4}$$

A single metric bulk horizontal relative diffusivity K_E, combining both x and y dispersion, is calculated from the time derivative of the ellipse area,

$$K_E(t) = \frac{1}{2}\frac{dD_E^2}{dt}, \tag{5}$$

where derivatives are estimated as forward Euler differences. Although dispersion does not scale as $D_E^2 \sim t$ over the tracking period (see section 3.1) and K_E is not constant, K_E is called a bulk horizontal diffusivity following previous relative dispersion studies (e.g., LaCasce, 2008). To minimize error in noisy estimates of K_E, a time-smoothing box car filter with linearly increasing span up to 24 hr is used before calculating the time derivative.

In the vertical (z), the relevant statistic is absolute dispersion as the sea surface is adjacent to the release location (e.g., Clark et al., 2010; Spydell & Feddersen, 2012a). The absolute vertical dispersion D_{zz}^2 is defined as

$$D_{zz}^2(t) = \langle \Delta z(t)^2 \rangle, \tag{6}$$

where Δz is the drifter displacement from its release location. A corresponding vertical diffusivity K_z is defined analogous to the horizontal diffusivity (5).

3. Results

A snapshot of drifter positions at $t = 30$ hr for all 30-m isobath releases shows the initial center of mass and dispersal pattern in the NT, LT, and WT simulations (Figures 2a–2c). In all three simulations, the release center of mass (white circles, Figures 2a–2c) has migrated south and offshore of their initial location (white strip, Figure 2a), consistent with coastal upwelling. Drifters remain onshore of the shelf break (≈ 100-m isobath) and form alongshore-elongated patches, as in previous studies (e.g., Davis, 1985; Dever et al., 1998; Romero et al., 2013). In geographic coordinates, the alongshore-drifter dispersion in WT (Figure 2c) is larger than in NT or LT (Figures 2a and 2b).

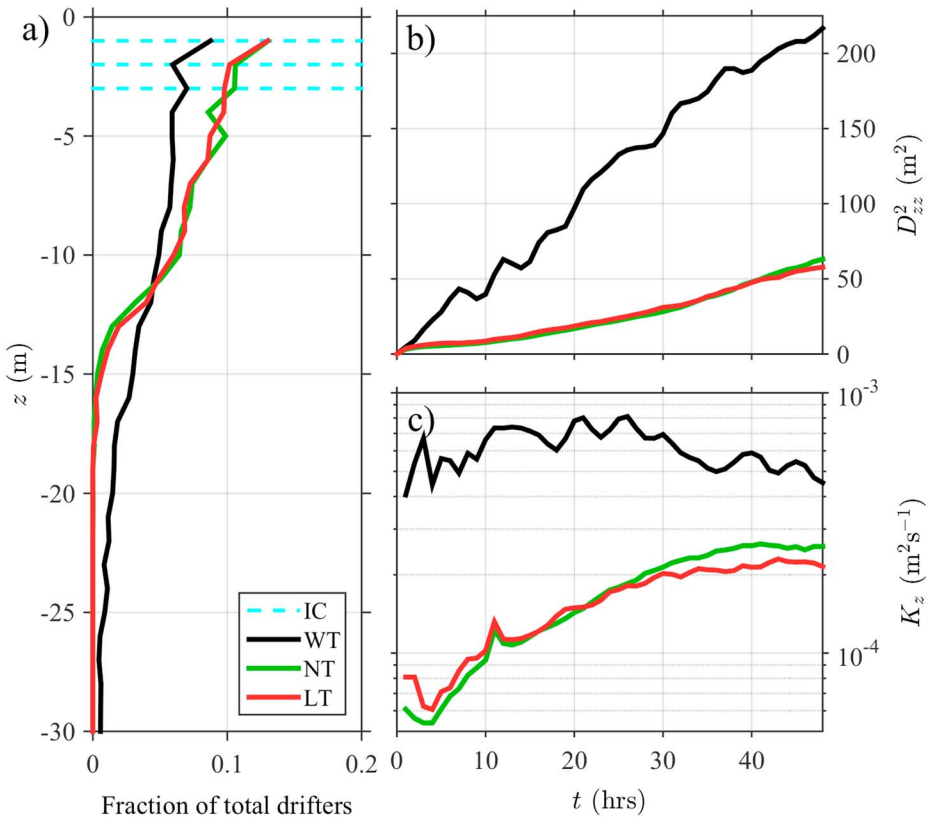

Figure 4. (a) Vertical drifter location probability distribution function at t = 30 hr after release from the 30-m isobath. The initial release locations at $z = -1, -2, -3$ m are indicated by dashed cyan lines and reach fractional value of 0.33. (b) Vertical drifter dispersion D_z^2 and (c) one half its time derivative analogous to equation (5) versus time after drifter release. The WT, NT, and LT simulation line colors are indicated in legend (panel a). WT = with tides; NT = no tides; LT = local tides.

3.1. Horizontal Relative Dispersion

In all three simulations with 30-m isobath releases, the relative dispersion major axis is 3–4 times larger than the minor axis (Figures 2d–2f) at $t = 30$ hr. At this time, the bulk horizontal relative dispersion ellipse area D_E^2 (4) is very similar between NT and LT (Figures 2d and 2e). In contrast, the WT D_E^2 is about twice as large as NT and LT (Figure 2f). The drifter probability distribution in both x' and y' directions are similar in NT and LT (shaded curves, Figures 2d and 2e). The WT simulation probability distributions are significantly wider (Figure 2f) consistent with the larger D_E^2. Results are similar for the 50-m isobath release.

Time series of bulk horizontal ellipse area $D_E^2(t)$ (4) and bulk horizontal diffusivity $K_E(t)$ (5) further quantify the dispersion differences between WT, NT, and LT for 30- and 50-m isobath releases (Figure 3). For $t < 10$ hr, drifters occupy less than 3 km^2 (Figures 3a and 3b), with rapidly increasing K_E (Figures 3c and 3d) for both 30- and 50-m isobath releases in all simulations. For longer times (10–48 hr), D_E^2 and K_E continue increasing without reaching a constant K_E diffusive limit, as might be expected given the overall red velocity spectrum with strong diurnal and semidiurnal peaks in the BC and BT simulations (Suanda et al., 2017) and the coastline variability. Over the 48 hr, NT and LT D_E^2 and K_E are similar while WT D_E^2 and K_E are a factor of 2–3 times larger than NT and LT for both 30- and 50-m releases (Figure 3). The similarity between LT and NT horizontal dispersion statistics indicates that at this location BT tides only induce a weak increase in horizontal dispersion relative to the horizontal stirring in NT. In contrast, BC tides induce a 2–3 times increase in horizontal dispersion statistics. Note that the bulk horizontal diffusivity K_E due to the horizontal stirring of coastal eddies (NT) with tidal processes (LT and WT) is much greater than the LTRANS random walk horizontal diffusivity of $k_H = 1$ m^2/s (Figures 3c and 3d).

3.2. Vertical Drifter Dispersion

Increased horizontal dispersion in WT relative to NT and LT is also mirrored in the vertical drifter dispersion. At $t = 30$ hr the NT and LT vertical drifter distributions are similar (green and red lines, Figure 4a) having

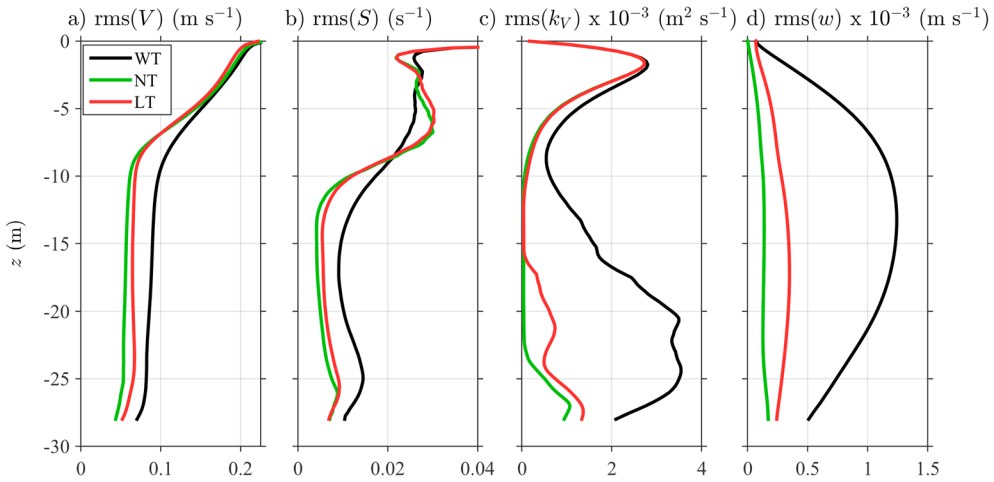

Figure 5. Vertical profiles of 30-m isobath root-mean-square (rms) Eulerian quantities: (a) rms horizontal velocity (a) ($V = (u^2 + v^2)^{1/2}$), (b) shear ($S = ((\partial_z u)^2 + (\partial_z v)^2)^{1/2}$), (c) rms model vertical eddy diffusivity (k_V), and (d) rms vertical velocity (w). The rms is calculated in both time between 1 July and 6 July and 20 km following the 30-m isobath latitude 34.9°N and 35.1°N. The bottom 2 m of the water column is masked due to tidal sea level fluctuations.

dispersed from their near-surface release ($-3 \le z \le -1$ m) down to about $z = -12$ m, with few drifters below $z = -15$ m. In contrast, the WT simulation has a smaller near-surface drifter fraction relative to NT and LT with substantial drifter fraction below $z = -15$ m (black line, Figure 4a). After 48 hr, drifter dispersion D_{zz}^2 is about 50 m^2 in NT and LT, whereas WT D_{zz}^2 is 4 times larger than NT and LT (Figure 4b). For WT, the vertical diffusivity K_z is fairly constant over the 48 hr (Figure 4c). The NT and LT K_z are similar, initially increasing and becoming approximately constant for $t > 30$ hr (Figure 4c), suggesting that BT tides do not have a large effect on the vertical dispersion of near-surface released drifters. For $t < 24$ hr, the WT K_z is a factor of 5–10 times larger than the LT and NT K_z. For longer times ($t > 40$ hr), the WT K_z is a factor of 2–2.5 times larger than LT and NT. Thus, BC tides in this region also significantly increase drifter vertical dispersion.

3.3. Eulerian Profiles

Root-mean-square (rms) Eulerian profiles of horizontal speed ($V = (u^2+v^2)^{1/2}$), shear ($S = ((\partial_z u)^2+(\partial_z v)^2)^{1/2}$), vertical velocity w, and model vertical eddy diffusivity k_V (Figure 5) are examined to understand differences between WT, NT, and LT horizontal and vertical drifter dispersion. Here the rms is taken through both time (5-day period, 1–6 July) and space (20 km following the 30-m isobath) and includes both tidal and subtidal time scales. The vertical profiles of rms(V; Figure 5a) and rms (S; Figure 5b) are not strongly affected by the presence of BT or BC tides, although the WT rms(V) and rms(S) are elevated a factor of about 1/3 over LT and NT in the lower water column ($z < -10$ m). With drifters concentrated in the upper water column, this suggests that increased WT horizontal dispersion is not due to horizontal stirring alone. In all three simulations, model rms(k_V) are generally similar in the upper 10 m (Figure 5c) as wind-driven processes dominate near-surface mixing (e.g., Allen et al., 1995; Austin & Lentz, 2002; Wijesekera et al., 2003) and are not significantly modified by BT or BC tides (Suanda et al., 2017). This 10-m thick surface layer roughly corresponds to the depth reached by NT and LT drifters after 30 hr (Figure 4a). Note that in this upper layer the rms(k_V) are dominated by the time mean. Below $z = -10$ m, WT rms(k_V) is larger than NT or LT due to increased shear from dissipating BC tides (Suanda et al., 2017). Throughout the water column, WT rms(w) is significantly (4–5 times) larger than in the NT and LT simulations (Figure 5d). The WT rms(w) vertical profile has midwater column maximum, similar to the expected structure of a mode-1 BC tide. The additional vertical stirring provided by WT rms(w) together with the subsurface enhanced WT rms(k_V) induces increased vertical drifter dispersion relative to NT and LT (Figure 4).

4. Discussion

4.1. Shear Dispersion Due to Coastal BC Tides

Horizontal dispersion in the NT and LT simulations is due to horizontal stirring by coastal eddies on length scales spanning 1–10 km (Figure 2). As the WT, NT, and LT simulations have largely similar near-surface ($z > -10$ m) rms horizontal velocities (Figure 5a), horizontal stirring is likely similar and cannot explain the increased WT horizontal dispersion. For WT, the increased vertical velocity and mixing with sheared and slightly stronger horizontal currents potentially induce additional horizontal dispersion through shear

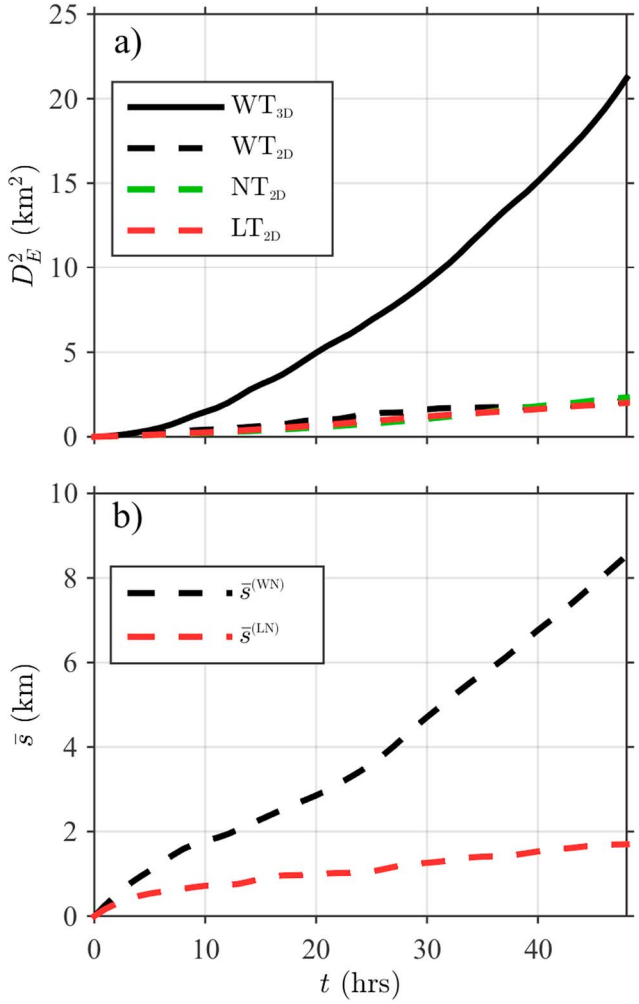

Figure 6. (a) Horizontal relative dispersion ellipse area D_E^2 versus time after drifter release from the $z = -1$ m, 50-m isobath. Two methods of drifter tracking are from the full 3-D velocity field and vertical mixing (WT_{3D}, solid black) and the 2-D surface horizontal velocity only (WT_{2D}, NT_{2D}, and LT_{2D}, dashed). The WT, NT, and LT simulation line colors are indicated in legend. (b) Ensemble separations $\bar{s}^{(WN)}$ (7) and $\bar{s}^{(LN)}$ versus time after drifter release from the 50-m isobath for 2-D tracking. WT = with tides; NT = no tides; LT = local tides.

dispersion (e.g., Steinbuck et al., 2011; Young et al., 1982). Classic, bounded vertical shear dispersion (e.g., Taylor, 1953), an asymptotic state with vertically uniform drifter distribution (i.e., strong mixing), has long-time horizontal diffusivity inversely proportional to the constant vertical absolute diffusivity. This result also applies for a vertical diffusivity with a finite Lagrangian time scale (Spydell & Feddersen, 2012b). However, for shear dispersion in an unbounded fluid (Saffman, 1962) or with weak mixing (Young et al., 1982), horizontal diffusivity increases with vertical mixing, similar to the K_E and K_z results here over 48 hr.

For the 30-m isobath release, the near-surface released WT drifters are concentrated in the upper half of the water column (Figure 4a) and $D_{zz}^2 < h^2$ over 48 hr (Figure 4b), indicating no influence of the lower boundary. Furthermore, Young et al. (1982) introduce a nondimensional parameter $k^* = K_z m^2/\omega$ to distinguish strong ($k^* \gg 1$) and weak ($k^* \ll 1$) mixing regimes, where m and ω are the vertical wavenumber and frequency of oscillatory shear, respectively. Applied to the WT simulation at the 30-m isobath, the $t = 48$ hr WT vertical diffusivity is $K_z = 4.7 \times 10^{-4}$ m^2/s (section 3.2) and a mode 1 semidiurnal (12.42-hr period) internal tide has $m = \pi/h = 0.1$ rad/m and $\omega = 1.4 \times 10^{-4}$ rad/s. This yields $k \ast= 0.03$, indicating a weak mixing regime where horizontal dispersion increases with vertical dispersion. This is consistent with the larger horizontal and vertical dispersion in the WT simulation relative to NT and LT.

4.2. Evolution of Near-Surface Trapped Drifters

Three-dimensional (3-D) drifter evolution is not important for all coastal tracers. For example, search-and-rescue or oil-spill response applications (e.g., Spaulding et al., 2006; Thyng & Hetland, 2017) require knowledge of surface-trapped (2-D) horizontal relative dispersion statistics and accurate drifter trajectory realizations. As vertical shear dispersion enhances WT bulk horizontal dispersion, this raises the question of whether including BT and BC tides is similarly important to accurately represent the evolution of surface-trapped drifters. To address this question, the $z = -1$-m near-surface released drifters are horizontally (2-D) advected, maintaining a constant z level, denoted (for WT) WT_{2D}, and 3-D tracking is denoted WT_{3D} (and similarly for NT and LT).

Over 48 hr, WT_{2D}, NT_{2D}, and LT_{2D} have similar bulk horizontal ellipse area D_E^2 reaching $\approx$ 2 km at 48 hr (Figure 6a). This indicates that, over 48 hr, near-surface trapped 2-D relative dispersion is not affected by BT or BC tides in this region. Furthermore, over the 48 hr $WT_{3D} D_E^2$ is significantly (8 times) larger than for WT_{2D}, NT_{2D}, and LT_{2D} (Figure 6a). This is consistent with the WT_{3D} strongly influenced by shear dispersion. Thus, in this region, BC and BT tides can be neglected for application that requires near-surface trapped relative dispersion statistics only.

In contrast to the relative dispersion statistics estimated from a single model simulation, a separation statistic across different simulations is constructed to examine BT and BC tide influence on individual drifter trajectories. The difference in drifter trajectories across simulations is quantified with the ensemble separation statistic $\bar{s}^{(WN)}$ (between WT_{2D} and NT_{2D}),

$$\bar{s}^{(WN)}(t) = \left\langle [(\Delta x^{(WN)}(t))^2 + (\Delta y^{(WN)}(t))^2]^{1/2} \right\rangle , \tag{7}$$

where $\Delta x^{(WN)}(t)$ and $\Delta y^{(WN)}(t)$ are the time-dependent east-west and north-south drifter separations between WT_{2D} and NT_{2D} simulations, respectively, and the ensemble average $\langle \cdot \rangle$ is over all drifter trajectories and releases. The ensemble LT_{2D} and NT_{2D} separation $\bar{s}^{(LN)}$ is similarly defined. Note that the $\bar{s}^{(WN)}$ statistic is not a dispersion metric. The WT_{2D} and NT_{2D} ensemble separation $\bar{s}^{(WN)}$ grows with time, from $\bar{s}^{(WN)} = 3$ km at $t = 24$ hr to $\bar{s}^{(WN)} = 8$ km at $t = 48$ hr (black, Figure 6b). In contrast, $\bar{s}^{(LN)}$ is much smaller than $\bar{s}^{(WN)}$, reaching only $\bar{s}^{(LN)} = 2$ km at $t = 48$ hr (red, Figure 6b). Thus, the substantial drifter trajectory difference between WT_{2D} and NT_{2D}

is due to BC tides, as regional BC tidal currents are twice as strong as BT tidal currents (Buijsman et al., 2011; Suanda et al., 2017). Simulations that neglect BC tides will result in large trajectory errors for specific applications (search and rescue) in this region. Different regions a have different mix of BC, BT, and subtidal currents which will govern the size of trajectory errors when neglecting BC or BT tides. However, for accurate trajectory realizations, the sources and phasings of BC tides must be accurately simulated, which is challenging as coastal BC tides have multiple sources (e.g., Buijsman et al., 2011; Suanda & Barth, 2015) with unpredictable phasing (Nash et al., 2012).

5. Summary

The effects of BT and BC tides on coastal drifter dispersion are examined with realistic high-resolution Central Californian shelf simulations. During coastal upwelling, for 3-D tracked drifters over 48 hr, the horizontal relative dispersion and vertical dispersion are similar between simulations with NT and with BT tides. In contrast, BC tides induce a factor of 2–3 times larger horizontal dispersion and about a factor of 2 times larger vertical dispersion through increased vertical velocities and subsurface model vertical diffusivity. Here the k-ϵ turbulence closure model is able to respond to increased shear from dissipating BC tides to increase subsurface model vertical diffusivity.

The increase in horizontal dispersion with vertical mixing is qualitatively consistent with weak-mixing shear dispersion. For surface-trapped (2-D) drifters, horizontal relative dispersion is similar in the WT, NT, and LT simulations and much weaker than the horizontal dispersion in WT with 3-D tracking. In contrast, after 48 hr drifter trajectory differences between simulations with NT and BC tides are 8 km, much larger than horizontal relative dispersion estimates from an individual model. This suggests the importance of BC tides for search-and-rescue or oil-spill response applications. These results apply to the Central Californian continental shelf region and require accurate BC tide predictions. Other regions have different relative strengths of BC and BT tides, which will affect their relative importance on coastal dispersion with both 3-D tracking and 2-D tracking.

Acknowledgments
S. H. S. acknowledges the National Science Foundation support through OCE-1521653. We gratefully acknowledge support from the Office of Naval Research award N00014-15-1-260 (F. F.) and N00014-17-1-2890 (N. K.). We thank Arthur Miller, Emanuele DiLorenzo, Kevin Haas, Donghua Cai, and Chris Edwards for their support in the modeling effort. Many helpful conversations with colleagues from the ONR Inner-Shelf Departmental Research Initiative are also appreciated. In accordance with AGU policy, model results and plotting tools are available at https://sandbox.zenodo.org/record/219504#.W7aDHlOFMnc. Please email ata.suanda@otago.ac.nz for further details.

References

Allen, J. S., Newberger, P. A., & Federiuk, J. (1995). Upwelling circulation on the Oregon continental shelf. Part I: Response to idealized forcing. *Journal of Physical Oceanography*, *25*(8), 1843–1866. https://doi.org/10.1175/1520-0485(1995)025

Austin, J. A., & Lentz, S. J. (2002). The inner shelf response to wind-driven upwelling and downwelling. *Journal of Physical Oceanography*, *32*(7), 2171–2193. https://doi.org/10.1175/1520-0485(2002)032

Boehm, A. B., Sanders, B. F., & Winant, C. D. (2002). Cross-shelf transport at Huntington Beach. Implications for the fate of sewage discharged through an offshore ocean outfall. *Environmental Science & Technology*, *36*(9), 1899–1906. https://doi.org/10.1021/es0111986

Bracco, A., Choi, J., Kurian, J., & Chang, P. (2018). Vertical and horizontal resolution dependency in the model representation of tracer dispersion along the continental slope in the northern Gulf of Mexico. *Ocean Modelling*, *122*, 13–25. https://doi.org/10.1016/j.ocemod.2017.12.008

Buijsman, M. C., Uchiyama, Y., McWilliams, J. C., & Hill-Lindsay, C. R. (2011). Modeling semidiurnal internal tide variability in the Southern California Bight. *Journal of Physical Oceanography*, *42*(1), 62–77. https://doi.org/10.1175/2011JPO4597.1

Chao, Y., Farrara, J. D., Zhang, H., Armenta, K. J., Centurioni, L., Chavez, F., et al. (2017). Development, implementation, and validation of a California coastal ocean modeling, data assimilation and forecasting system. *Deep Sea Research Part II: Topical Studies in Oceanography*, *151*, 49–63. https://doi.org/10.1016/j.dsr2.2017.04.013

Clark, D. B., Feddersen, F., & Guza, R. T. (2010). Cross-shore surfzone tracer dispersion in an alongshore current. *Journal of Geophysical Research*, *115*, C10035. https://doi.org/10.1029/2009JC005683

Cowen, R. K., & Sponaugle, S. (2009). Larval dispersal and marine population connectivity. *Annual Review of Marine Science*, *1*, 443–466.

Dale, A. C., Levine, M. D., Barth, J. A., & Austin, J. A. (2006). A dye tracer reveals cross-shelf dispersion and interleaving on the Oregon shelf. *Geophysical Research Letters*, *33*, L03604. https://doi.org/10.1029/2005GL024959

Davis, R. E. (1983). Oceanic property transport, Lagrangian particle statistics, and their prediction. *Journal of Marine Research*, *41*(1), 163–194. https://doi.org/10.1357/002224083788223018

Davis, R. E. (1985). Drifter observations of coastal surface currents during CODE: The statistical and dynamical views. *Journal of Geophysical Research*, *90*(C3), 4756–4772. https://doi.org/10.1029/JC090iC03p04756

Davis, R. E. (1991). Lagrangian ocean studies. *Annual Review of Fluid Mechanics*, *23*(1), 43–64.

Dever, E. P., Hendershott, M. C., & Winant, C. D. (1998). Statistical aspects of surface drifter observations of circulation in the Santa Barbara Channel. *Journal of Geophysical Research*, *103*(C11), 24,781–24,797. https://doi.org/10.1029/98JC02403

Drake, P. T., Edwards, C. A., & Barth, J. A. (2011). Dispersion and connectivity estimates along the U.S. West Coast from a realistic numerical model. *Journal of Marine Research*, *69*(1), 1–37. https://doi.org/10.1357/002224011798147615

Durski, S. M., Glenn, S. M., & Haidvogel, D. B. (2004). Vertical mixing schemes in the coastal ocean: Comparison of the level 2.5 Mellor-Yamada scheme with an enhanced version of the K profile parameterization. *Journal of Geophysical Research*, *109*, C01015. https://doi.org/10.1029/2002JC001702

Ganju, N. K., Lentz, S. J., Kirincich, A. R., & Farrar, J. T. (2011). Complex mean circulation over the inner shelf south of Martha's Vineyard revealed by observations and a high-resolution model. *Journal of Geophysical Research*, *116*, C10036. https://doi.org/10.1029/2011JC007035

Haidvogel, D. B., Arango, H., Budgell, W. P., Cornuelle, B. D., Curchitser, E., Di Lorenzo, E., et al. (2008). Ocean forecasting in terrain-following coordinates: Formulation and skill assessment of the regional ocean modeling system. *Journal of Computational Physics*, *227*(7), 3595–3624. https://doi.org/10.1016/j.jcp.2007.06.016

Hally-Rosendahl, K., Feddersen, F., & Guza, R. T. (2014). Cross-shore tracer exchange between the surfzone and inner-shelf. *Journal of Geophysical Research: Oceans*, *119*, 4367–4388. https://doi.org/10.1002/2013JC009722

Hodur, R., Hong, X., Doyle, J., Pullen, J., Cummings, J., Martin, P., & Rennick, M. A. (2002). The coupled ocean/atmosphere mesoscale prediction system (COAMPS). *Oceanography*, *15*(1), 88–98. https://doi.org/10.5670/oceanog.2002.39

Jullien, M.-C., Paret, J., & Tabeling, P. (1999). Richardson pair dispersion in two-dimensional turbulence. *Physical Review Letters*, *82*, 2872–2875.

Kelly, S. M., Jones, N. L., Nash, J. D., & Waterhouse, A. F. (2013). The geography of semidiurnal mode-1 internal-tide energy loss. *Geophysical Research Letters*, *40*, 4689–4693. https://doi.org/10.1002/grl.50872

Kim, S., & Barth, J. A. (2011). Connectivity and larval dispersal along the Oregon coast estimated by numerical simulations. *Journal of Geophysical Research*, *116*, C06002. https://doi.org/10.1029/2010JC006741

Kumar, N., Feddersen, F., Suanda, S., Uchiyama, Y., & McWilliams, J. (2015). Mid- to inner-shelf coupled ROMS-SWAN model-data comparison of currents and temperature: Diurnal and semidiurnal variability. *Journal of Physical Oceanography*, *46*(3), 841–862. https://doi.org/10.1175/JPO-D-15-0103.1

Kunze, E., & Sundermeyer, M. A. (2015). The role of intermittency in internal-wave shear dispersion. *Journal of Physical Oceanography*, *45*(12), 2979–2990. https://doi.org/10.1175/JPO-D-14-0134.1

Kurapov, A. L., Erofeeva, S. Y., & Myers, E. (2017). Coastal sea level variability in the US West Coast Ocean Forecast System (WCOFS). *Ocean Dynamics*, *67*(1), 23–36. https://doi.org/10.1007/s10236-016-1013-4

LaCasce, J. H. (2008). Statistics from Lagrangian observations. *Progress in Oceanography*, *77*(1), 1–29. https://doi.org/10.1016/j.pocean.2008.02.002

Lacorata, G., Palatella, L., & Santoleri, R. (2014). Lagrangian predictability characteristics of an Ocean Model. *Journal of Geophysical Research: Oceans*, *119*, 8029–8038. https://doi.org/10.1002/2014JC010313

MacKinnon, J. A., & Gregg, M. C. (2003). Shear and baroclinic energy flux on the summer New England shelf. *Journal of Physical Oceanography*, *33*(7), 1462–1475.

Macfadyen, A., Watabayashi, G. Y., Barker, C. H., & Beegle-Krause, C. J. (2011). Tactical modeling of surface oil transport during the deepwater horizon spill response. In Y. Liu, A. MacFadyen, Z.-G. Ji, & R. H. Weisberg (Eds.), *Monitoring and Modeling the Deepwater Horizon Oil Spill: A Record-Breaking Enterprise* (271 pp.). Washington, DC: American Geophysical Union. https://doi.org/10.1029/2011GM001128

Marchesiello, P., McWilliams, J. C., & Shchepetkin, A. (2001). Open boundary conditions for long-term integration of regional oceanic models. *Ocean Modelling*, *3*(1), 1–20.

Mark, D. J., Spargo, E. A., Westerink, J. J., & Luettich, R. A. (2004). ENPAC 2003: A tidal constituent database for eastern North Pacific Ocean (Tech. Rep. ERDC/CHL-TR-04-12). Washington, DC: Coastal and Hydraul. Lab., U.S Army Corps of Eng.

Mason, E., Molemaker, J., Shchepetkin, A. F., Colas, F., McWilliams, J. C., & Sangra, P. (2010). Procedures for offline grid nesting in regional ocean models. *Ocean Modelling*, *35*(1-2), 1–15. https://doi.org/10.1016/j.ocemod.2010.05.007

McPhee-Shaw, E. (2006). Boundary-interior exchange: Reviewing the idea that internal-wave mixing enhances lateral dispersal near continental margins. *Deep Sea Research Part II: Topical Studies in Oceanography*, *53*(1-2), 42–59. https://doi.org/10.1016/j.dsr2.2005.10.018

Mitarai, S., Siegel, D. A., Watson, J. R., Dong, C., & McWilliams, J. C. (2009). Quantifying connectivity in the coastal ocean with application to the Southern California Bight. *Journal of Geophysical Research*, *114*, C10026. https://doi.org/10.1029/2008JC005166

Monismith, S. G., Barkdull, M. K., Nunome, Y., & Mitarai, S. (2018). Transport between Palau and the Eastern Coral Triangle: Larval connectivity or near misses. *Geophysical Research Letters*, *45*, 4974–4981. https://doi.org/10.1029/2018GL077493

Moniz, R. J., Fong, D. A., Woodson, C. B., Willis, S. K., Stacey, M. T., Monismith, S. G., et al. (2014). Scale-dependent dispersion within the stratified interior on the shelf of Northern Monterey Bay, https://doi.org/10.1175/JPO-D-12-0229.1

Nash, J. D., Kelly, S. M., Shroyer, E. L., Moum, J. N., & Duda, T. F. (2012). The unpredictable nature of internal tides on continental shelves. *Journal of Physical Oceanography*, *42*(11), 1981–2000. https://doi.org/10.1175/JPO-D-12-028.1

North, E. W., Hood, R. R., Chao, S. Y., & Sanford, L. P. (2006). Using a random displacement model to simulate turbulent particle motion in a baroclinic frontal zone: A new implementation scheme and model performance tests. *Journal of Marine Systems*, *60*(3), 365–380. https://doi.org/10.1016/j.jmarsys.2005.08.003

Ohlmann, J. C., LaCasce, J. H., Washburn, L., Mariano, A. J., & Emery, B. (2012). Relative dispersion observations and trajectory modeling in the Santa Barbara Channel. *Journal of Geophysical Research*, *117*, C05040. https://doi.org/10.1029/2011JC007810

Ohlmann, J. C., & Mitarai, S. (2010). Lagrangian assessment of simulated surface current dispersion in the coastal ocean. *Geophysical Research Letters*, *37*, L17602. https://doi.org/10.1029/2010GL044436

Paduan, J. D., & Niiler, P. P. (1993). Structure of velocity and temperature in the northeast Pacific as measured with Lagrangian drifters in fall 1987. *Journal of Physical Oceanography*, *23*(4), 585–600. https://doi.org/10.1175/1520-0485(1993)023<0585:SOVATI>2.0.CO;2

Petersen, C. H., Drake, P. T., Edwards, C. A., & Ralston, S. (2010). A numerical study of inferred rockfish (Sebastes spp.) larval dispersal along the central California coast. *Fisheries Oceanography*, *19*(1), 21–41. https://doi.org/10.1111/j.1365-2419.2009.00526.x

Pineda, J., Hare, J. A., & Sponaugle, S. (2007). Larval transport and dispersal in the coastal ocean and consequences for population connectivity. *Oceanography*, *20*(3), 22–39.

Poje, A. C., Özgökmen, T. M., Lipphardt, L., Haus, B. K., Ryan, E. H., Haza, A. C., et al. (2014). Submesoscale dispersion in the vicinity of the Deepwater Horizon spill. *Proceedings of the National Academy of Sciences*, *111*(35), 12,693–12,698. https://doi.org/10.1073/pnas.1402452111

Rasmussen, L. L., Cornuelle, B. D., Levin, L. A., Largier, J. L., & Di Lorenzo, E. (2009). Effects of small-scale features and local wind forcing on tracer dispersion and estimates of population connectivity in a regional scale circulation model. *Journal of Geophysical Research*, C01012. https://doi.org/10.1029/2008JC004777

Rayson, M. D., Gross, E. S., Hetland, R. D., & Fringer, O. B. (2016). Time scales in Galveston Bay: An unsteady estuary. *Journal of Geophysical Research: Oceans*, *121*, 2268–2285. https://doi.org/10.1002/2015JC011181

Richardson, L. F. (1926). Atmospheric diffusion shown on a distance-neighbour graph. *Proceedings of the Royal Society of A*, *110*, 709–737.

Romero, L., Uchiyama, Y., Ohlmann, J. C., McWilliams, J. C., & Siegel, D. A. (2013). Simulations of nearshore particle-pair dispersion in Southern California. *Journal of Physical Oceanography*, *43*(9), 1862–1879. https://doi.org/10.1175/JPO-D-13-011.1

Rypina, I. I., Kirincich, A., Lentz, S., & Sundermeyer, M. (2016). Investigating the eddy diffusivity concept in the coastal ocean. *Journal of Physical Oceanography*, *46*(7), 2201–2218. https://doi.org/10.1175/JPO-D-16-0020.1

Saffman, P. G. (1962). The effect of wind shear on horizontal spread from an instantaneous ground source. *Quarterly Journal of the Royal Meteorological Society*, *88*(378), 382–393. https://doi.org/10.1002/qj.49708837803

Salazar, J. P., & Collins, L. R. (2009). Two-particle dispersion in isotropic turbulent flows. *Annual Review of Fluid Mechanics*, *41*(1), 405–432. https://doi.org/10.1146/annurev.fluid.40.111406.102224
Sawford, B. (2001). Turbulent relative dispersion. *Annual Review of Fluid Mechanics*, *33*(1), 289–317. https://doi.org/10.1146/annurev.fluid.33.1.289
Schlag, Z., & North, E. W. (2012). Lagrangian TRANSport (LTRANS) v.2 model user's guide (Technical Report). Cambridge, MD: University of Maryland Center for Environmental Science Horn Point Laboratory.
Shchepetkin, A. F., & McWilliams, J. C. (2005). The regional oceanic modeling system (ROMS): A split-explicit, free-surface, topography-following-coordinate oceanic model. *Ocean Modelling*, *9*(4), 347–404. https://doi.org/10.1016/j.ocemod.2004.08.002
Spaulding, M. L., Isaji, T., Hall, P., & Allen, A. (2006). A hierarchy of stochastic particle models for search and rescue (SAR): Application to predict surface drifter trajectories using HF radar current forcing. *Journal of Marine Environmental Engineering*, *8*(3), 181.
Spydell, M., & Feddersen, F. (2009). Lagrangian drifter dispersion in the surf zone: Directionally spread, normally incident waves. *Journal of Physical Oceanography*, *39*(4), 809–830.
Spydell, M. S., & Feddersen, F. (2012a). A Lagrangian stochastic model of surf zone drifter dispersion. *Journal of Geophysical Research*, *117*, C03041. https://doi.org/10.1029/2011JC007701
Spydell, M. S., & Feddersen, F. (2012b). The effect of a non-zero Lagrangian time-scale on bounded shear dispersion. *Journal of Fluid Mechanics*, *691*, 69–94. https://doi.org/10.1017/jfm.2011.433
Spydell, M. S., Feddersen, F., & Guza, R. T. (2009). Observations of drifter dispersion in the surfzone: The effect of sheared alongshore currents. *Journal of Geophysical Research*, *114*, C07028. https://doi.org/10.1029/2009JC005328
Steinbuck, J. V., Jeffrey, K. R., Amatzia, G., Mark, S. T., & Stephen, M. G. (2011). Horizontal dispersion of ocean tracers in internal wave shear. *Journal of Geophysical Research*, *116*, C11031. https://doi.org/10.1029/2011JC007213
Suanda, S. H., & Barth, J. A. (2015). Semidiurnal baroclinic tides on the central Oregon inner shelf. *Journal of Physical Oceanography*, *45*(10), 2640–2659. https://doi.org/10.1175/JPO-D-14-0198.1
Suanda, S. H., Feddersen, F., & Kumar, N. (2017). The effect of barotropic and baroclinic tides on coastal stratification and mixing. *Journal of Geophysical Research: Oceans*, *122*, 10,156–10,173. https://doi.org/10.1002/2017JC013379
Suanda, S. H., Kumar, N., Miller, A. J., Di Lorenzo, E., Haas, K., Cai, D., et al. (2016). Wind relaxation and a coastal buoyant plume north of Pt. Conception, CA: Observations, simulations, and scalings. *Journal of Geophysical Research: Oceans*, *121*, 7455–7475. https://doi.org/10.1002/2016JC011919
Sundermeyer, M. A., & Ledwell, J. R. (2001). Lateral dispersion over the continental shelf: Analysis of dye release experiments. *Journal of Geophysical Research*, *106*(C5), 9603–9621. https://doi.org/10.1029/2000JC900138
Taylor, G. I. (1922). Diffusion by continuous movements. *Proceedings of the London Mathematical Society*, *s2-20*(1), 196–212. https://doi.org/10.1112/plms/s2-20.1.196
Taylor, G. I. (1953). Dispersion of soluble matter in solvent flowing slowly through a tube. *Proceedings of the Royal Society of London A*, *219*, 186–203.
Thyng, K. M., & Hetland, R. D. (2017). Texas and Louisiana coastal vulnerability and shelf connectivity. *Marine pollution bulletin*, *116*(1-2), 226–233.
Umlauf, L., & Burchard, H. (2005). Second-order turbulence closure models for geophysical boundary layers. A review of recent work. *Continental Shelf Research*, *25*(78), 795–827. https://doi.org/10.1016/j.csr.2004.08.004
Veneziani, M., Edwards, C. A., Doyle, J. D., & Foley, D. (2009). A central California coastal ocean modeling study: 1. Forward model and the influence of realistic versus climatological forcing. *Journal of Geophysical Research*, *114*, C04015. https://doi.org/10.1029/2008JC004774
Walter, R. K., Woodson, C. B., Arthur, R. S., Fringer, O. B., & Monismith, S. G. (2012). Nearshore internal bores and turbulent mixing in southern Monterey Bay. *Journal of Geophysical Research*, *117*, C07017. https://doi.org/10.1029/2012JC008115
Warner, J. C., Armstrong, B., He, R., & Zambon, J. B. (2010). Development of a Coupled Ocean-Atmosphere-Wave-Sediment Transport (COAWST) modeling system. *Ocean Modelling*, *35*(3), 230–244. https://doi.org/10.1016/j.ocemod.2010.07.010
Warner, J. C., Sherwood, C. R., Arango, H. G., & Signell, R. P. (2005). Performance of four turbulence closure models implemented using a generic length scale method. *Ocean Modelling*, *8*(1-2), 81–113. https://doi.org/16/j.ocemod.2003.12.003
Wijesekera, H. W., Allen, J. S., & Newberger, P. A. (2003). Modeling study of turbulent mixing over the continental shelf: Comparison of turbulent closure schemes. *Journal of Geophysical Research*, *108*(C3), 3103. https://doi.org/10.1029/2001JC001234
Wunsch, C. (1971). Note on some Reynolds stress effects of internal waves on slopes. *Deep Sea Research and Oceanographic Abstracts*, *18*(6), 583–591. https://doi.org/10.1016/0011-7471(71)90124-0
Young, W. R., Rhines, P. B., & Garrett, C. J. R. (1982). Shear-flow dispersion, internal waves and horizontal mixing in the ocean. *Journal of Physical Oceanography*, *12*(6), 515–527. https://doi.org/10.1175/1520-0485(1982)012